

RESEARCH

Open Access



Seismic Retrofitting of RC Circular Columns Using Carbon Fiber, Glass Fiber, or Ductile PET Fiber

Donguk Choi¹, Seongwon Hong^{2*}, Myung-Kwan Lim³, Sang-Su Ha⁴ and Sorrasak Vachirapanyakun⁵

Abstract

The effectiveness of seismic retrofitting using three different fibers—carbon fiber (CF), glass fiber (GF), polyethylene terephthalate (PET) fiber—and a fiber combination of aramid fiber (AF) and PET fiber (called hybrid fiber reinforced polymer (HF)) wrapped on reinforced concrete (RC) circular columns was experimentally evaluated. A total of 11 RC circular columns were tested: three control columns and eight retrofitted columns in three different test groups. The purpose of fiber wrapping was flexural strength improvement as well as enhancement of rotational capacity in the plastic hinge region. Mechanical properties of CF, GF, AF, and PET were first defined; that is, CF, GF, and AF exhibited linear stress–strain behavior with limited ultimate strain capacity typically less than 3%, while ductile PET exhibited as much as 15% strain and non-linear stress–strain behavior with a very low elastic modulus. In the RC column tests, all three different fibers and the AF + PET fiber combination were effective in enhancing the strength and ductility but resulted in different structural behaviors and failure modes depending on the fiber type and the fiber amount used. The column sections were then analytically studied by section analysis using the behavior of confined concrete, the non-linear relationship of fiber-reinforced polymer (FRP), and the actual material properties of reinforcement. The analytical and experimental results revealed that ductile PET is beneficial, as it demonstrates more ductile behavior with a degree of strength enhancement similar to that of CF and GF.

Keywords: Axial stiffness, Confined concrete, Ductile fiber, Hybrid fiber, Section analysis

1 Introduction

For many existing reinforced concrete (RC) building columns and bridge piers designed and constructed in the 1960s and 1970s in many countries, including South Korea, there is a need to increase flexural and shear capacities, as well as ductility. Fiber reinforced polymer (FRP) wrapping using carbon fiber (CF) and glass fiber (GF) has been widely employed and successfully completed for retrofitting RC columns, which have insufficient flexural strength and ductility for seismic actions.

Although CF is an excellent material with high strength, high elastic modulus, and excellent durability, it has its own deficiencies, such as high cost, very small rupture strain of about 1%, and electric conductivity. GF is more economical than CF and has good strength and elastic modulus, but it also has deficiencies, including a small rupture strain smaller than 3%, and its performance may not be reliable when exposed to certain environmental conditions, such as alkalinity, moisture, and ultra violet. Aramid fiber (AF) is also an excellent material with mechanical properties between CF and GF and has good durability, but its rupture strain is about 3% (ACI, 2003; ACI, 2007).

Recently, some researchers have focused on the use of new fibers with high to very high ultimate strain in tension, such as polyethylene naphthalate (PEN) and

*Correspondence: shong@ut.ac.kr

² Department of Safety Engineering, Korea National University of Transportation, Chungju, Chungbuk, Korea

Full list of author information is available at the end of the article
Journal Information: ISSN 1976-0485 / EISSN 2234-1315

polyethylene terephthalate (PET), for seismic retrofitting of RC columns (Anggawidjaja et al., 2006; Dai et al., 2012; Fahmy & Wu, 2010; Liu & Li, 2018; Liu & Sheikh, 2013; Mirmiran et al., 1998; Saleem et al., 2018; Ueda et al., 2006; Zhang et al., 2017; Obaidat et al., 2021) PET and PEN have a large rupture strain and good strength, but the elastic modulus is low for both fibers. The stress-strain behaviors of both fibers are non-linear. On the weight-based comparison, PET is more economical than PEN.

Anggawidjaja et al. (2006) used FRP such as PEN and PET with large fracture strain for seismic retrofit of RC columns. Through an experimental study of 15 shear-deficient square RC piers, they concluded that RC piers wrapped by multiple PET or PEN layers with large fracture strain could efficiently enhance the ductility of RC piers, and PET and PEN could be used for shear strengthening of RC piers lacking transverse reinforcement if an adequate amount of fiber is provided, regardless of their low stiffness. They also proposed an analytical model to predict the pier's deformation capacity based on the experimental results. Liu and Sheikh (2013) conducted tests on nine reinforced concrete circular columns subjected to simulated seismic loads. The specimens were designed with a wide-space steel spiral, and eight specimens were retrofitted with FRP. The test results showed that FRP confinement effectively improved the seismic resistance of columns but displayed different characteristics from steel-confined columns. Curvature ductility and the energy dissipation capacity of a section increased with an increase in FRP confinement. Youssf et al. (2015) conducted a parameter study using LS-DYNA to investigate the plastic hinge length for FRP wrapped RC columns. Parghi and Alam (2017) performed nonlinear static pushover analysis to study influencing parameters including concrete strength, yielding strength of rebar, amount of longitudinal steel rebar, level of axial load, shear span-depth ratio, and carbon FRP confinement layer for RC bridge piers retrofitted with FRP. Zhang et al. (2017) performed experiments to examine the influence of stirrup corrosion on the shear contribution of a PET-FRP sheet and substrate columns wrapped by PET. The shear resistance of the PET-wrapped RC square columns was enhanced by the volume ratio of the PET sheet at the peak load and decreased as the corrosion level of the stirrups increased. Based on the test results, a prediction model was proposed to capture the shear capacity of corroded RC columns strengthened by PET-FRP sheet. In 2018, Liu and Li (2018) investigated the seismic behavior of corroded RC square and circular columns wrapped with carbon FRP sheets and PET-600 composites. To corrode the steel bar, the electrochemical corrosion method was used with 15% of corrosion rate. It was concluded

that PET-600 and CFRP had anti-seismic capacity in terms of hysteretic hoops, failure modes, residual displacement, stiffness degradation, damping ratio, and energy dissipation. Saleem et al. (2018) studied the lateral response of PET-confined concrete with circular, square, or rectangular cross sections using small-scale specimens. A total of 54 specimens were tested under monotonic axial compression, while test variables were cross-sectional shape, corner radius (in the case of square or rectangular sections), and number of PET layers. In circular specimens, the PET's large strain capacity was utilized to enhance the strength and lateral ductility of confined concrete. In square and rectangular specimens with low effective confinement, PET mainly contributed to recovering strength loss, while in sufficiently confined specimens, it also resulted in significant strength gain, with a significant increase in lateral ductility. In 2019, Cao and Pham provided the guideline for determining CFRP/GFRP for confinement retrofitting of RC structures poorly confined based on experimental study. Naser et al. (2019) reviewed the FRP composites and summarized the state-of-the-art experimental, analytical, and numerical works involving FRPs applied to infrastructures including building. Mhanna et al. (2020) investigated the mechanical properties of PET FRP in terms of thermal effect and developed temperature-dependent models. To investigate the effectiveness of CFRP, seismic-retrofit tests of circular RC bridge piers were carried out by Zhou et al. (2021). The authors clearly showed that CFRP can reduce vulnerability under lateral loading, and a semi-empirical model for maximum displacement was successfully proposed based on the test data. Although there are many studies for FRP to strengthen RC columns, at present there is no strong consensus in the literature on seismic retrofitting of existing RC columns using various FRPs, such as CF, GF, and PET. Based on the authors' knowledge, few large-scale laboratory tests have been performed on tied RC circular columns wrapped with PET FRP.

The purpose of this study was to experimentally and analytically compare the structural performance of columns retrofitted by different fibers or fiber combinations in terms of strength and ductility improvement using three different types of fibers (CF, GF, and PET) and one fiber combination (AF/PET, called hybrid fiber reinforced polymer (HF)) for seismic retrofitting of RC columns by fiber wrapping. The study's main emphasis was to identify the behavior of the PET-strengthened columns and draw comparisons on the behavior of the RC columns strengthened by relatively new ductile fibers with the behaviors of the columns confined by more conventional CF- and AF- strengthened columns. A total of 11 columns were tested in 3 test groups (TGs): 3 control columns and 8 retrofitted columns. The test scheme

was pseudo-dynamic lateral reverse cyclic loading with constant axial force simulating seismic action. The main purpose of retrofitting was to improve flexural capacity and ductility in the plastic hinge region. The stress–strain behavior of concrete confined by different fibers was then analytically investigated using an existing model. Section analyses were performed to construct moment–curvature diagrams, including the material properties of confined concrete, reinforcing steel, FRP, and adhesive used in the experiment. The analytical investigation concentrated on the confinement effect of different fibers or fiber combinations, which should be directly related to strength and ductility improvement.

The importance of this research is as follows:

- This study compares the behavior of RC columns externally wrapped by various FRP systems, such as Carbon FRP, Aramid FRP, and PET FRP, and subjected to reverse cyclic loading.
- This study provides rare information on the confinement effect of tied RC circular columns using PET FRP.
- The hybrid strand constructed in this study using AF and PET is the first attempt at hybridization of ductile PET and conventional fiber (such as AF) to increase stiffness and constructability.

2 Experimental program

2.1 Fibers

The mechanical properties of the various fibers used in this study were determined following ISO 10406-2 (ISO, 2015), with the results shown in Table 1 and Fig. 1. Tensile strength, ultimate strain in tension, and elastic modulus of CF, GF, AF, and PET measured in this study agree well with those available in the literature (ACI, 2003). It was observed that the ultimate strain of PET was about

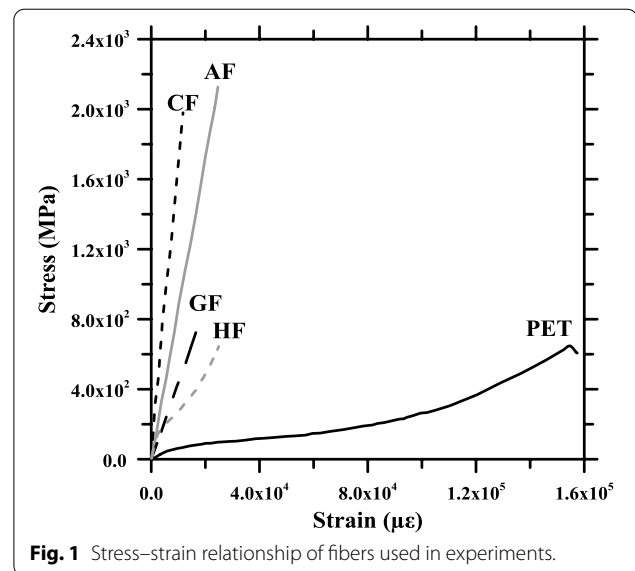


Fig. 1 Stress–strain relationship of fibers used in experiments.

15%, whereas its strength was almost comparable to that of GF. While the stress–strain relationship of CF, GF, and AF was linear, PET exhibited a highly non-linear stress–strain relationship. Due to the non-linearity of PET, a reference value of 1% strain was selected as the secant modulus of elasticity of PET. In Fig. 1, HF denotes a special hybridized fiber that consists of AF and PET (the design of the HF strand is explained in detail in Sect. 3.1.2). The mechanical properties in tension of the two-part epoxy used in this study, determined by ASTM D 638 (ASTM, 2008), are also provided in Table 1.

2.2 Test Variables

Eleven RC circular columns were tested in three different test groups (TG). TG-1 consisted of a control column, a CF wrapped column (1 layer of CF sheet), and a PET wrapped column (20 layers of PET sheet). TG-2 was

Table 1 Material properties of fibers and adhesive

Fiber type	Density g/mm ³	Thickness mm	Cross-sectional area mm ²	Tensile strength MPa	Max. strain in tension	Elastic modulus MPa	Stress–strain behavior
CF roving	0.00180	–	0.446	1,970	0.0116	169,000	Linear
GF roving	0.00254	–	0.970	788	0.0176	44,800	Linear
AF roving	0.00144	–	0.109	2126	0.0243	87,400	Linear
PET sheet ¹	0.00140	0.106	5.250	613	0.1495	7100	Non-linear
AF/PET (HF) strand ²	–	1.317	132.000	630	0.1540	–	Non-linear
Epoxy	–	–	–	40.9	0.0258	1586	Linear

CF is carbon fiber; GF is glass fiber; AF is aramid fiber; PET is polyethylene terephthalate

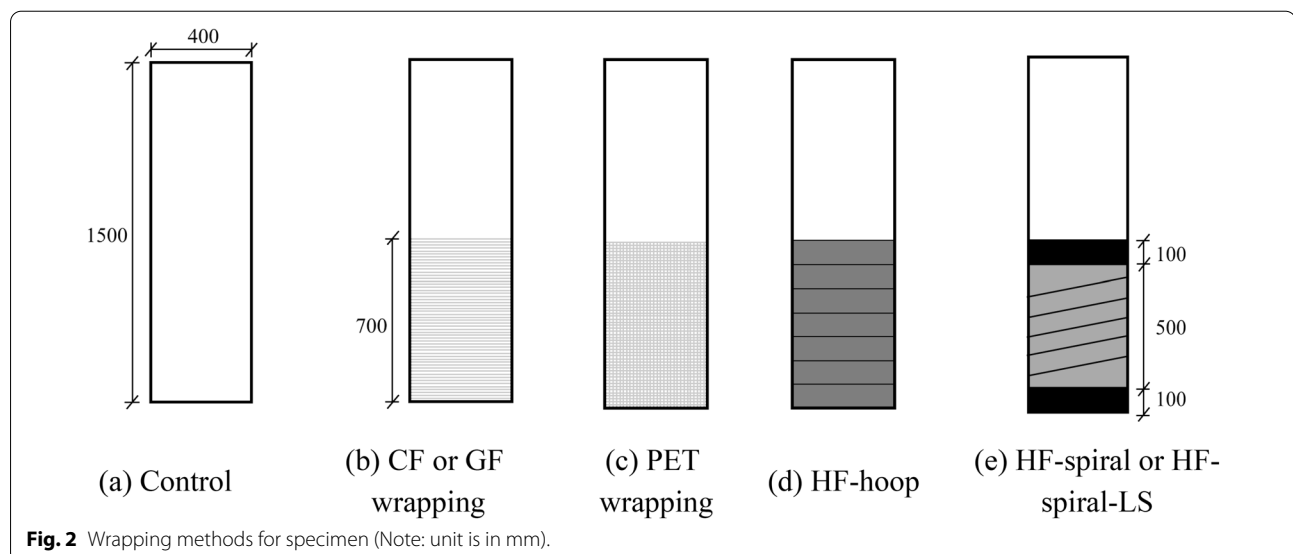
¹ Cross-sectional area for bi-axially-woven PET sheet is given for axial direction only per 100 mm width; ² AF/PET hybrid strand consists of 120.8 mm² PET and 10.9 mm² AF per 100 mm width

composed of a control column, a GF wrapped column (1 layer of GF sheet), and a PET wrapped column (10 layers of PET sheet). TG-3 consisted of a control column, a PET wrapped column (25 layers of PET sheet), and three HF wrapped columns (1 layer of HF strand wrapped in the form of a hoop or spiral, respectively, in addition to a column with lap-spliced main bars and a spiral strengthening scheme using HF). Uniaxial CF and GF sheets were made of CF or GF rovings with material properties similar to those summarized in Table 1. The PET sheet used in this study was bi-axially woven and is often used as geotextile fabric. TG-1 and TG-2 tests were prepared to compare the effectiveness of the column retrofitting by fiber wrapping between fibers with small ultimate strain versus fibers with large strain capacity, that is, CF versus ductile PET in TG-1 and GF versus ductile PET in TG-2. TG-3 tests compared the effectiveness of HF versus multiple layers of PET wrapping. Fig. 2 and 3 show the wrapping methods of the specimens and their pictures, respectively.

Table 2 summarizes the test variables, including concrete strength, steel reinforcement ratio, fiber reinforcement ratio, fiber type, number of fiber wrappings, and method of application. As the main purpose of the fiber wrapping was to improve flexural capacity and ductility in the plastic hinge region in this study, the fibers were applied only in the lower part of the columns, where the moment was at the maximum. We observed that the control columns were not designed as shear critical and were, therefore, expected to fail in flexure or flexure–shear. In all TGs, the axial stiffness

of the FRPs was similar between FRP strengthened columns in each TG; that is, the axial stiffness of CF one layer and PET 20 layers, GF one layer and PET 10 layers, and HF one layer and PET 25 layers were approximately the same in each TG (see Table 2).

RC columns were typically designed using materials often used in the 1970s and 1980s. Low-to-normal-strength concretes were supplied from a ready-mixed concrete plant. Compression test cylinders with a diameter of 100 mm and a height of 200 mm were prepared, and three cylinders were tested at the ages of 7, 28, and 56 days. Strength changes after 56 days would be very small when the columns were tested, and compressive strengths at 56 days, shown in Table 2, were used for the interpretation of the test results and analyses. Table 3 displays the mechanical properties of steel reinforcement. TG-1 RC columns used low-strength concrete ($f_{cu}=21.0$ MPa) and Grade SD300 deformed reinforcing bars ($f_y=347$ MPa). Twelve D16 evenly positioned rebars along the perimeter were used as the main reinforcement in a circular section in TG-1. TG-2 and TG-3 RC columns used normal strength concrete ($f_{cu}=30.8$ MPa and 41.4 MPa, respectively, for TG-2 and TG-3, and Grade SD400 rebars (12 D16 with $f_y=403$ MPa and 8 D19 with $f_y=454$ MPa, respectively, for TG-2 and TG-3). Column ties were Grade SD400 D10 rebars with $f_y=465$ MPa. Same rebars were used as column ties, while the spacing was 250 mm and 300 mm at the center for TG-1 and TG-2 and for TG-3, respectively. All material properties of reinforcing steel, summarized in Table 3, were measured by the authors in the laboratory using proper instruments, including 1200-kN capacity Instron 4495 UTM and strain gauges.



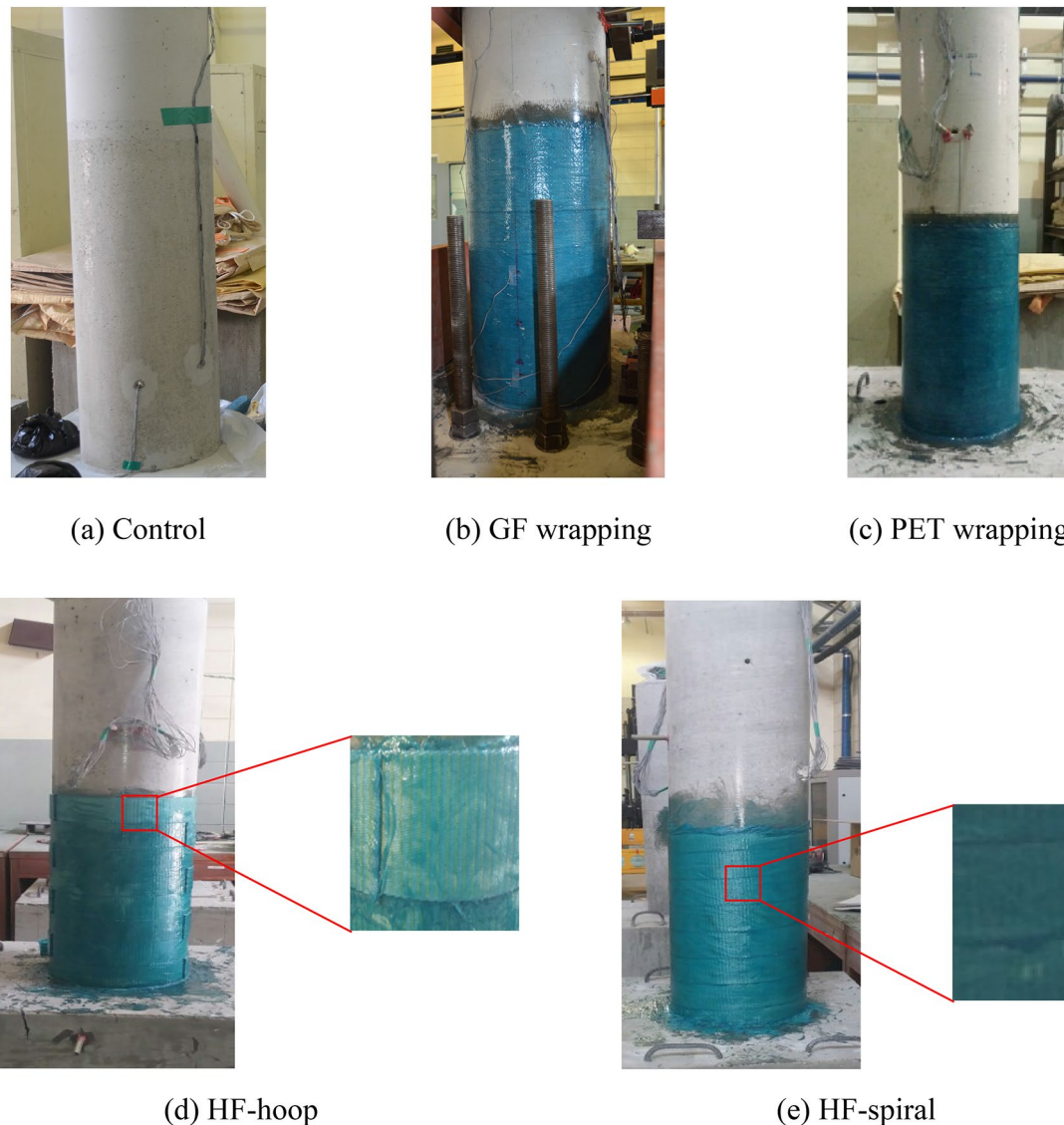


Fig. 3 Control specimen and fibers wrapped specimens.

2.3 Preparation for Test and Test Procedures

The RC columns were cast in two parts: a column stub and column. Column stub ($1200 \times 1000 \times 600$ mm) was first made using 40-MPa normal strength concrete and a large amount of reinforcement to make sure that failure occurred in the column during the test without any cracking or deformation of the stub. The hooked end of the column's main reinforcing bars was set in the stub, while the straight bars extended into the column without any lap splicing, as shown in Fig. 4. About a week after casting the stub, the column was cast. With 400 mm of diameter and 1500 mm of height of the circular column representing half-length of a column with fixed

conditions at both ends, the specimens can be considered as 2/3 scale of the real column. After the column stubs and columns were cast and cured, the surface of the lower part of the columns was lightly roughened using a hand grinder and then cleaned using a vacuum cleaner for a height of about two times the effective depth ($2d$) (see Figs. 2 and 3). Sufficient amount of two-part epoxy was used for fiber wrapping, while the adhesive amount was 200% of fibers by volume. All fibers were wrapped manually around the column. The columns were tested at least 56 days after the specimen fabrication was completed.

All specimens were fabricated and tested at the Structural Laboratory of Hankyong National University. A

Table 2 Column index, concrete strength, steel/fiber reinforcement ratios and fiber wrapping scheme.

TG	Specimen index	f_{cu} MPa	ρ_{st} %	ρ_{tie} %	ρ_f %	Fiber type	# of layers	Method of application [Area of fiber (mm ² /pitch)]
1	C-1-Control	21.0	1.93	0.37	–	–	–	–
	C-1-CF				0.108	CF	1	CF sheet (27.23)
	C-1-PET				1.05	PET	20	PET sheet (262.5)
2	C-2-Control	30.8	1.93	0.37	–	–	–	–
	C-2-GF				0.108	GF	1	GF sheet (106)
	C-2-PET				1.05	PET	10	PET sheet (132)
3	C-3-Control	41.1	1.83	0.29	–	–	–	–
	C-3-PET				1.31	PET	25	PET sheet (393.8)
	C-3-HF-hoop				1.32	HF	1	HF strand, hoop (PET = 362.4&AF = 32.7)
	C-3-HF-spiral				1.32	HF	1	HF strand, spiral (PET = 362.4&AF = 32.7)
	C-3-HF-spiral-LS				1.32	HF	1	HF strand, spiral-LS (PET = 362.4&AF = 32.7)

LS is lap-splice (equal to 1.3 times development length); f_{cu} is compressive strength of concrete at 56 days; ρ_{st} is steel reinforcement ratio (A_{st}/A_g); A_{st} is area of steel; A_g is gross area of specimen; ρ_{tie} = tie reinforcement ratio (V_{tie}/V_{core_con}); V_{tie} is volume of column tie; V_{core_con} is volume of core concrete; ρ_f = fiber reinforcement ratio (V_f/V_{core_con}); V_f is volume of fiber (= area of fiber (mm²/pitch) × perimeter × pitch (1 pitch is 250 mm and 300 mm for TG-1 & TG-2 and TG-3, respectively; shear span (a) is 1,200 mm and 1250 mm for TG-1&TG-2 and TG-3, respectively; effective depth (d) is 352 mm for all columns; $a/d = 3.4$ and 3.5 for TG-1&TG-2 and TG-3, respectively; column diameter = 400 mm and column height = 1500 mm for all columns.

Table 3 Mechanical properties of deformed steel reinforcement

	Use	Series	Reinforcement	f_y MPa	f_u MPa	E_s MPa
Column	Main bar	1	12 D16	347	522	178,000
		2	12 D16	403	480	175,000
		3	8 D19	454	573	189,000
	Column tie	1, 2	D10 @ 250 mm o.c	465	718	181,000
		3	D10 @ 300 mm o.c			
Column stub	Main bar	1, 2, 3	D25	548	–	–
	Ties		D10	465	–	–

f_y is specified yield strength of reinforcement; f_u is tensile strength of reinforcement; E_s is young's modulus of reinforcement

1000-kN capacity actuator with ± 120 mm stroke was used to apply reverse cyclic lateral force at 1200 mm and 1250 mm of height above the stub top surface for TG-1 and TG-2, and TG-3, respectively, whereas a 2,000-kN hydraulic cylinder was used on top of the column to apply axial compression force simulating dead load during test (see Fig. 5). Using a set of hinges located on two sides of the column, it was possible to keep the axial force constant at about 10% of the column's axial capacity for each column during the test.

Pseudo-dynamic tests were carried out generally following procedures suggested in ACI 374.2R-13. Displacement control for the lateral force application was adopted and is shown in Fig. 6. As shown in Fig. 6, the same displacement cycle was repeated twice. At the initiation of each test, the axial load was first applied using a hydraulic cylinder on top of the column. Force was monitored using a pressure transducer equipped with a hand pump that operated the hydraulic cylinder. Lateral load was then applied using a 1000-kN actuator for displacement control, following the guidelines of

ACI 374.2R (ACI, 2013). Lateral load was applied and increased until tension reinforcement reached the yield strain, and then the lateral load was reversed, such that the tension reinforcement at the opposite side reached the yield strain, while subsequent unloading completed a cycle. The maximum displacements in both directions recorded by the linear variable displacement transducers (LVDT) at the top of the column were averaged and defined as Δ_y . One loading stage consisted of two cycles. In the subsequent stages, the test continued with increasing displacement, such that the maximum displacement of a specific stage was $2\Delta_y$, $3\Delta_y$, $4.5\Delta_y$, $6\Delta_y$, $8\Delta_y$, and $10\Delta_y$. The test ended when the peak load in the current cycle dropped by more than 20% from the maximum load recorded during test. In one tests of TG-2, end of stroke of the actuator was reached during test. The test specimen was completely unloaded and then was subjected to monotonic loading to failure. This also happened during TG-3 tests as the RC columns were wrapped by ductile PET or HF. All test data were digitally retrieved and recorded. Test of a control

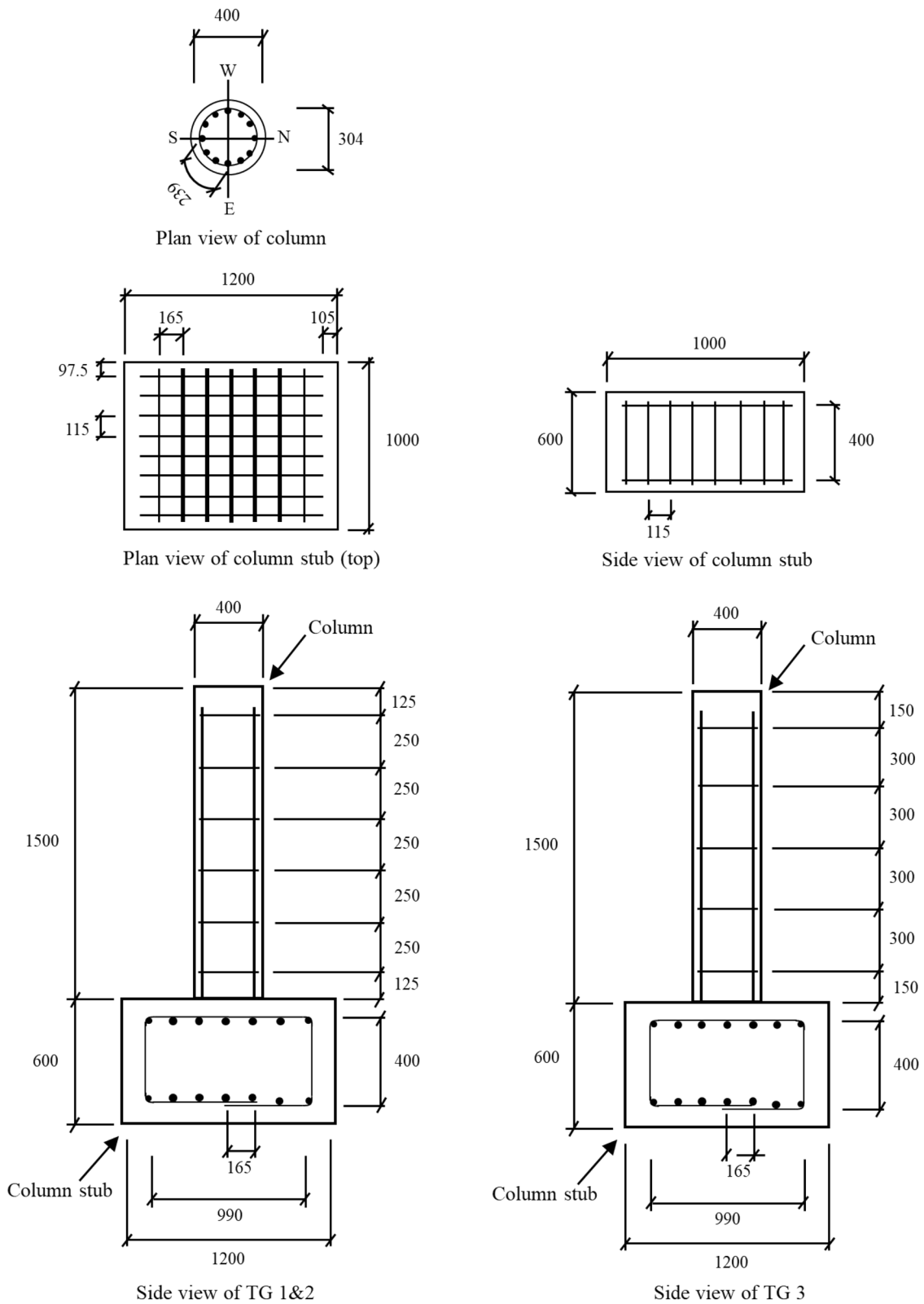


Fig. 4 Details of test specimens (Note: unit is in mm).

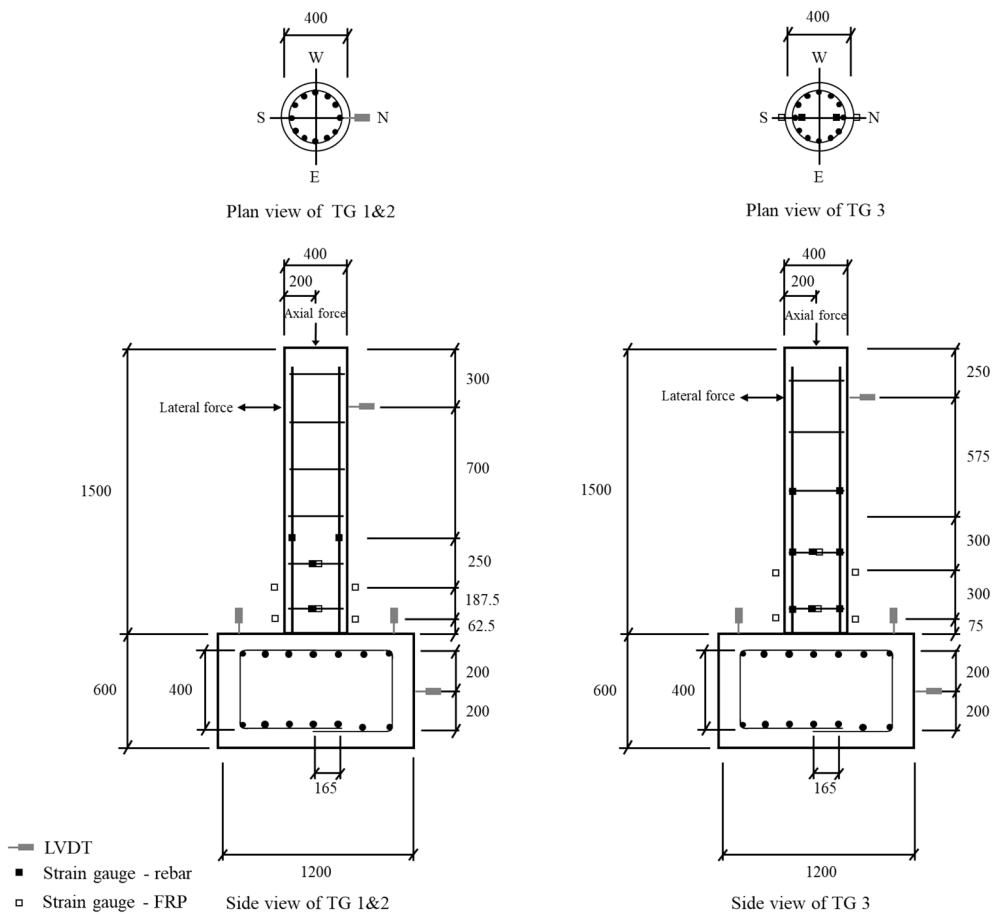
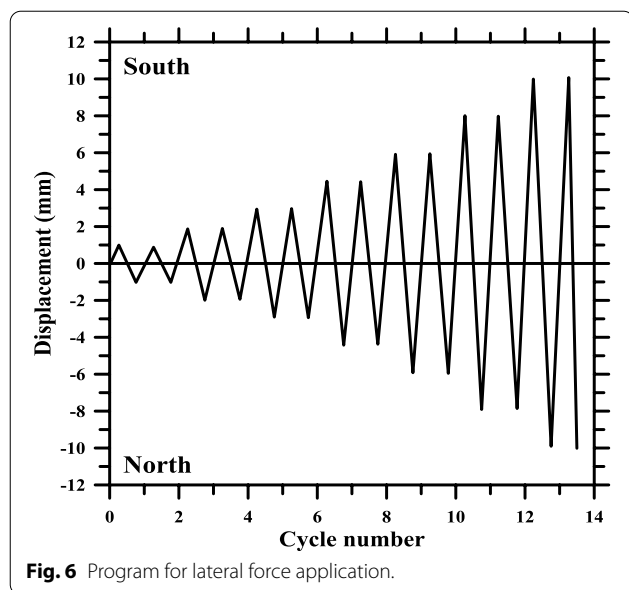


Fig. 5 Locations of vertical and horizontal loads, strain gauge, and LVDTs and a picture of setup (Note: unit is in mm).



column typically lasted for about 3 h, whereas testing a strengthened column lasted for about 5 h.

The column test specimens were heavily instrumented using strain gauges and LVDT, as shown in Fig. 5. An LVDT installed at 300 mm and 250 mm from the top of columns for TG-1 and TG-2, and TG-3, respectively, as the actuator was used to record column lateral displacement, two LVDTs set on the top surface of the stub were used to measure possible rigid body rotation of the stub, and two LVDTs at mid-height of the stub were used to measure horizontal rigid body translation of the stub, if any. Six sets of strain gauges were used on the column's main reinforcement located at the north end and south end, respectively, at half the distance between lower column ties. Four additional sets of strain gauges were used on column ties (first hoop and second hoop above top surface of stub) at the west and east ends to measure tie elongation in hoop direction. For retrofitted columns, four more strain gauges were used on the outer surface of fibers at the north and south ends at the same height as the strain gauges installed on the main reinforcement. Four additional strain gauges were installed on the east and west surfaces of the fibers at the first and second hoop levels, as shown in Fig. 5. It is noted that the north was the push direction, while the south was the pull direction during reverse cyclic loading.

3 Test results

3.1 Hysteretic Behavior

3.1.1 TG-1 and TG-2 Columns

Fig. 7a–c shows hysteretic behaviors of all TG-1 columns. Table 4 summarizes the test results for all columns. For

the C-1-Control, the yield load was 116 kN at 11.5 mm displacement. Load increased with increasing displacement, while the maximum load observed was 147 kN at 50.4 mm displacement, which corresponded to a 4.2% drift ratio, defined as the maximum displacement divided by the span length. Large concrete chunks spalled off at the same time as the buckling of the main bars at failure. The test terminated as the peak load dropped below 80% of the maximum load. For C-1-CF, which was retrofitted using a single layer of uniaxial CF sheet, the yield load was 126 kN with a displacement of 7.9 mm (drift ratio of 0.65%). The maximum load was 178 kN at 78.4 mm displacement (drift ratio of 6.5%). The final failure occurred in the next stage by sudden CF rupture, as shown in Fig. 8a, followed by main bar buckling. For C-1-PET, which was retrofitted using 20 layers of bi-axial PET sheet, the yield load was 130 kN at a displacement of 7.2 mm (drift ratio of 0.6%). The maximum load of 188 kN was reached at 96.1 mm displacement. Significant bulging of the PET was observed at the maximum load, as demonstrated in Fig. 8b. No rupture of ductile PET, however, was observed at the maximum load, and the final failure occurred at 96.1 mm displacement (drift ratio of 8.0%). As PET remained unruptured even after the final failure, part of the PET in the plastic hinge region was cut out after the end of the test, and the failure mode was investigated. It was found that the main bars buckled probably during the previous stage (or cycle), but the final failure was delayed until the next stage, when the buckled bars failed in tension during the subsequent loading cycle, as presented in Fig. 8c. Similar to the findings of a previous study by Liu and Li (2018), both the strength and ductility of the CF- and PET-retrofitted columns significantly increased compared to the control column. The maximum load of C-1-CF (1 layer of CF) increased by 21% compared to the control, and that of C-1-PET (20 layers of PET) increased by 28% compared to the control. C-1-PET also showed more ductile behavior in terms of the maximum displacement and drift ratio than C-1-CF. The final failure mode of the three TG-1 columns was concrete crushing and main bar buckling for C-1-Control, CF rupture at the maximum displacement for C-1-CF, and the main bar rupture in tension for C-1-PET.

Hysteretic behavior of all TG-2 columns is shown in Fig. 7d–f. The maximum load and the maximum displacement of C-2-GF and C-2-PET again increased significantly compared to the control column. For the C-2-Control, the maximum load was 157 kN at a displacement of 58.5 mm (drift ratio of 4.9%). For C-2-GF, the maximum load was 174 kN with a displacement of 98.0 mm (drift ratio of 8.2%). During the test, due to the limited stroke of the actuator, C-2-GF was unloaded

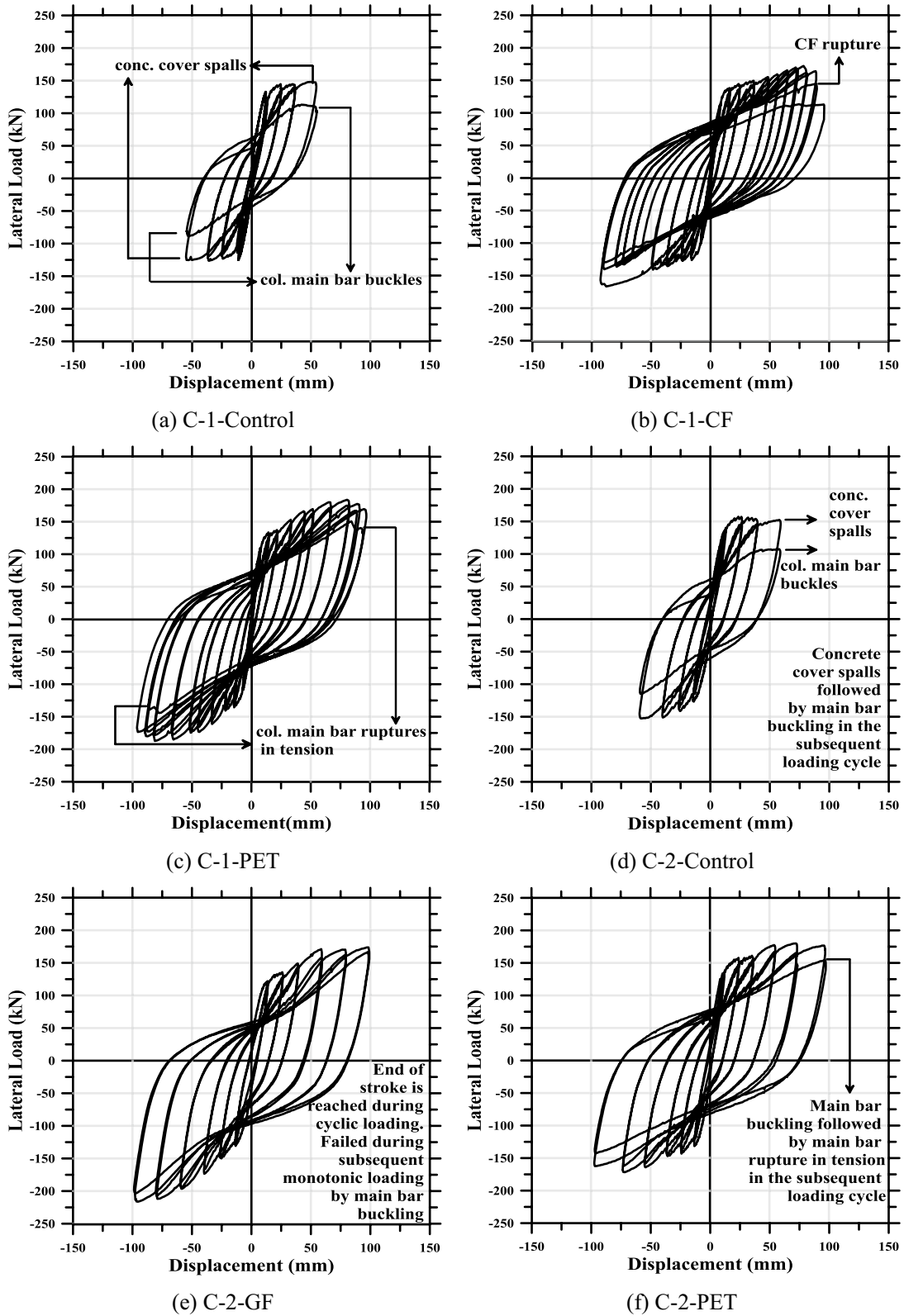


Fig. 7 Lateral load–displacement hysteretic responses.

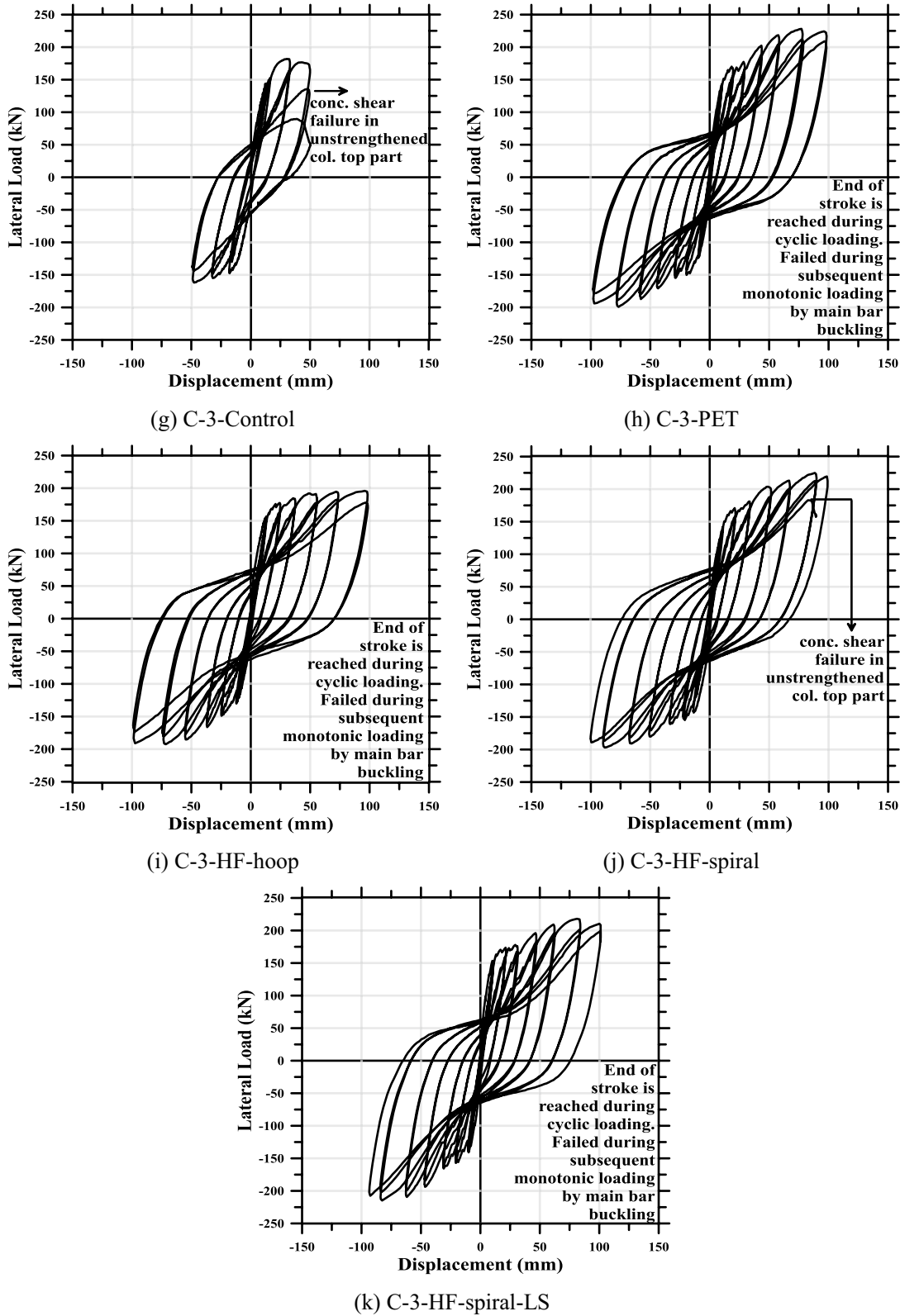
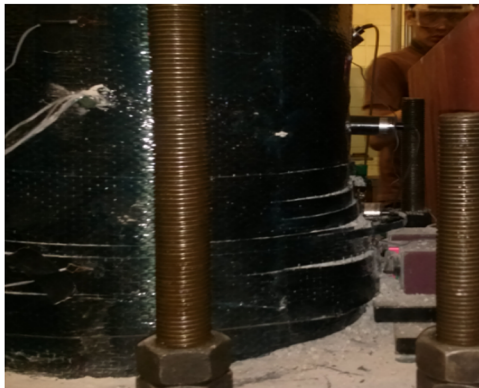


Fig. 7 continued

Table 4 Summary of column test results

Column index	Load		Displacement		Displacement ductility (mm)	Drift ratio (%)	Failure mode
	P_y (kNm)	P_{max} (kNm)	Δ_y (mm)	Δ_{max} (mm)			
C-1-Control	116	147	11.5	50.4	4.4	4.2	Main bar buckling
C-1-CF	126	178	7.9	78.4	9.9	6.5	CF rupture
C-1-PET	130	188	7.2	96.1	13.3	8.0	Main bar rupture
C-2-Control	134	157	11.3	58.5	5.2	4.9	Main bar buckling
C-2-GF	122	174 (222) ¹	13.7	98.0 (148) ¹	7.2 (10.8) ¹	8.2 (12.3) ¹	GF rupture
C-2-PET	134	180	10.6	96.0	9.1	8.0	Main bar rupture
C-3-Control	146	172	15.1	44.6	3.0	3.6	Shear failure
C-3-PET	133	214	9.6	83.3	8.7	6.7	Main bar rupture
C-3-HF-hoop	138	195	11.5	96.7	8.4	7.8	Main bar rupture
C-3-HF-spiral	133	211	10.9	88.4	8.1	7.1	Shear failure (upper part of column)
C-3-HF-spiral-LS	148	217	10.0	82.0	8.2	6.6	Shear failure (upper part of column)

P_y is yield load; P_{max} is the maximum load; Δ_y is yield displacement; Δ_{max} is displacement at the maximum load; ¹Monotonic loading



(a) C-1-CF (CF rupture)



(b) C-1-PET (PET bulging)



(c) C-1-PET (Bar failed in tension)

Fig. 8 Failure mode of CF and PET-strengthened TG-1 columns.

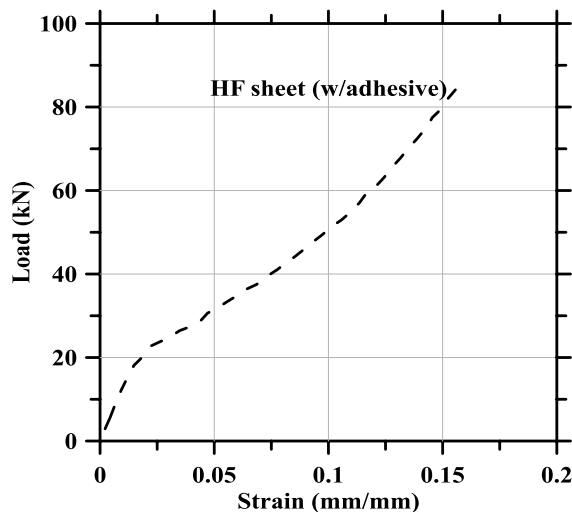
after the end of the reverse cyclic loading program and then monotonically loaded up to failure. The maximum load of 222 kN at 148 mm displacement was reached at failure, as shown in Table 4. Drift ratio was 12.3%. Final failure mode of C-2-GF was GF rupture followed by main bar buckling similar to C-1-CF. For the C-2-PET, the maximum load was 180 kN at a displacement of 96.0 mm. Drift ratio was 8.0% at failure. The failure mode of C-2-PET was similar to that of C-1-PET: that is, PET remained unruptured at failure, but the main bar first buckled and then ruptured in tension in the subsequent loading stage or cycle. TG-2 column test results again revealed that both the strength and ductility of the GF- and PET-strengthened columns significantly increased compared to the control column. The maximum load of C-2-GF (1 layer of GF) increased by 11% compared to the control during the reverse cyclic loading program, and that of C-2-PET (10 layers of PET) increased by 15% compared to the control. Both C-2-GF and C-2-PET showed ductile behavior in terms of displacement and drift ratio, as summarized in Table 4. The final failure mode of TG-2 columns was concrete crushing and main bar buckling for C-2-Control, GF rupture and main bar buckling for C-2-GF, and main bar rupture in tension for C-2-PET.

3.1.2 TG-3 Columns

TG-3 tests consisted of five test specimens, as described previously: a control column, a PET wrapped column, two specially fabricated HF strand wrapped columns, and an HF strand wrapped column with lap-spliced main

bars. In TG-1 and TG-2 tests, multiple layers (10 or 20 layers) of thin PET sheets had to be used, primarily due to the low elastic modulus of PET. As multiple layers of PET wrapping are labor-intensive (and thus not cost-effective), it was necessary to design and fabricate a fiber strand such that only one or two layers of strand wrapping would be necessary. In addition, mixing PET with low elastic modulus and other fibers with higher elastic modulus would confer a higher stiffness than a strand made of PET only (Choi et al., 2011). Aramid fiber (AF) was considered a proper fiber for this purpose because of its mechanical properties, such as high strength and elastic modulus and relatively large ultimate strain (see Table 1 and Fig. 1). HF strand was designed using principles of fiber mixing suggested by Manders and Bader (1981), and a strand with about 8% AF and 92% PET (by volume fraction) was fabricated. As the HF strand was put into tension, while AF ruptured first at about 3% strain, the strand tensile resistance was not decreased, but PET effectively continued to resist the tensile force. A typical load-versus-strain plot of the HF strand designed, fabricated, and used in this study is provided in Fig. 9. It was observed that an HF strand and 25 layers of PET had similar axial stiffness, that is, $E_f A_f$.

Fig. 7g–k presents the hysteretic behavior of five TG-3 columns: C-3-Control, C-3-PET, C-3-HF-hoop, C-3-HF-spiral, and C-3-HF-spiral-LS. C-3-PET was retrofitted by 25-layer PET wrapping, and C-3-HF-hoop and C-3-HF-spiral were wrapped with one layer of HF strand in a hoop direction and in spiral fashion, respectively, as schematically exhibited in Fig. 2d, e. For



(a) Load-strain behavior



(b) Tension test of HF strand in progress

Fig. 9 Load-strain behavior of HF strand in tension.

C-3-HF-hoop, each strand overlapped at the end for 100 mm length. For the C-3-HF-spiral, in which the HF strap was wrapped around continuously, it was necessary to wrap an extra hoop using the same strand at the top and bottom due to a detailing problem, as provided in Fig. 2e.

The test results described in Fig. 7g–k and Table 4 again revealed that all fiber wrapping schemes adopted in the TG-3 tests were effective, given that the maximum load, maximum displacement, and drift ratio improved significantly compared to the control. C-3-Control failed in shear at a 3.6% drift ratio, although the shear capacity was estimated to be higher than the flexural capacity before test. The maximum load of the C-3-Control was 172 kN. Higher maximum load of 214 kN was observed for C-3-PET. The maximum loads of C-3-HF-hoop, C-3-HF-spiral, and C-3-HF-spiral-LS were 195 kN, 211 kN, and 217 kN, respectively. Final failure mode of C-3-PET and C-3-HF-hoop was main bar rupture followed by main bar buckling (similar to C-1-PET), but C-3-HF-spiral and C-3-HF-spiral-LS failed by shear in the unstrengthened top part of column during reverse cyclic loading (see Fig. 7). Overall the performance of columns wrapped by one HF strand (C-3-HF-hoop, C-3-HF-spiral, and C-3-HF-spiral-LS) was similar to that of C-3-PET. We observed that there was no difference between the behaviors of C3-HF-Spiral (with straight main bars) and C3-HF-Spiral-LS (with lap-spliced main bars). Thus, it can be concluded that the HF strand served the intended purpose of improving the strength and drift ratio, as well as providing efficient retrofitting work.

3.2 Envelope, Stiffness, and Energy Dissipation

Fig. 10 shows envelopes of hysteretic curves, stiffnesses, and energy dissipation plots for all TG-1 and TG-2 columns. The stiffness was determined as the slope of a straight-line connecting origin and the peak of each cycle of the hysteretic curve, whereas the energy dissipation was defined as the area under one complete cycle (loop) of the hysteretic curve. For the TG-1 columns, the initial stiffness of the C-1-CF or C-1-PET was clearly higher than that of the control. For the TG-2 columns, the initial stiffness of the C-2-GF or C-2-PET column was also higher than that of the control column. The stiffness decreased with an increasing number of cycles (and hence with increasing displacements) for all columns. The energy dissipation plots of TG-1 show that more energy was dissipated by C-1-PET (20 layers of PET) than by C-1-CF (1 layer of CF). For TG-2, there were few differences in energy dissipation between C-1-GF (a layer of GF) and C-1-PET (10 layers of PET).

3.3 Hoop Strain

Fig. 11 shows the maximum hoop strains developed during the reverse cyclic loading in the column ties and on different fibers measured on the east and/or west side of the column section (see Fig. 5). In the TG-1 and TG-2 control columns, which are not designed as shear critical, the column ties did not develop a yield strain $\varepsilon_{yt} = 0.0025$ (see Table 3). For some retrofitted columns, the column ties yielded, for example, C-1-CF. Although C-3-Control was not designed as shear critical, it actually failed in shear, as described previously, with a maximum tie strain of 0.0054, significantly larger than the tie yield strain. In C-3-PET and C-3-HF-hoop, the maximum tie strains registered were smaller than the yield strain at the measured locations (i.e., strain gauge locations), but it can be assumed that the maximum tie strains were larger elsewhere and the ties actually yielded. After the ties were yielded, the fibers immediately kicked in to help resist shear, and so the fibers developed larger strain values. For C-3-PET and C-3-HF-hoop, the maximum fiber strains measured were 0.012 and 0.019, respectively, as shown in Fig. 11c.

Fig. 12 shows the maximum hoop strain values reached on extreme compression fibers for the retrofitted columns. For C-1-CF, the CF ruptured at a maximum strain of 1.3%. Much higher maximum hoop strain of 3.5% was registered for C-1-PET, but the ductile PET did not fail. For C-2-GF, again it can be assumed that the maximum hoop strain larger than that shown in Fig. 12 must have developed at a location other than the measured location as the GF ruptured during test. C-3-HF-hoop yielded the largest hoop strain registered, with a hoop strain of 7.7%, which clearly demonstrated the advantage of using ductile fibers, as PET did not rupture at the very large strains.

4 Analyses

Following the experimental program, section analyses were conducted to construct moment–curvature diagrams of the RC column sections tested. The purpose was to determine the effectiveness of different FRPs in increasing the strength and drift ratio in the retrofitted columns. The section analyses included the material properties of the confined concrete, reinforcing steel, FRP, and adhesives actually used in the experiment.

4.1 Stress Versus Strain of Confined Concrete

There are many existing models with which the theoretical stress–strain behavior of confined concrete can be determined. In this study, a well-known model by Mander et al. (1988) was adopted, as the model is excellent

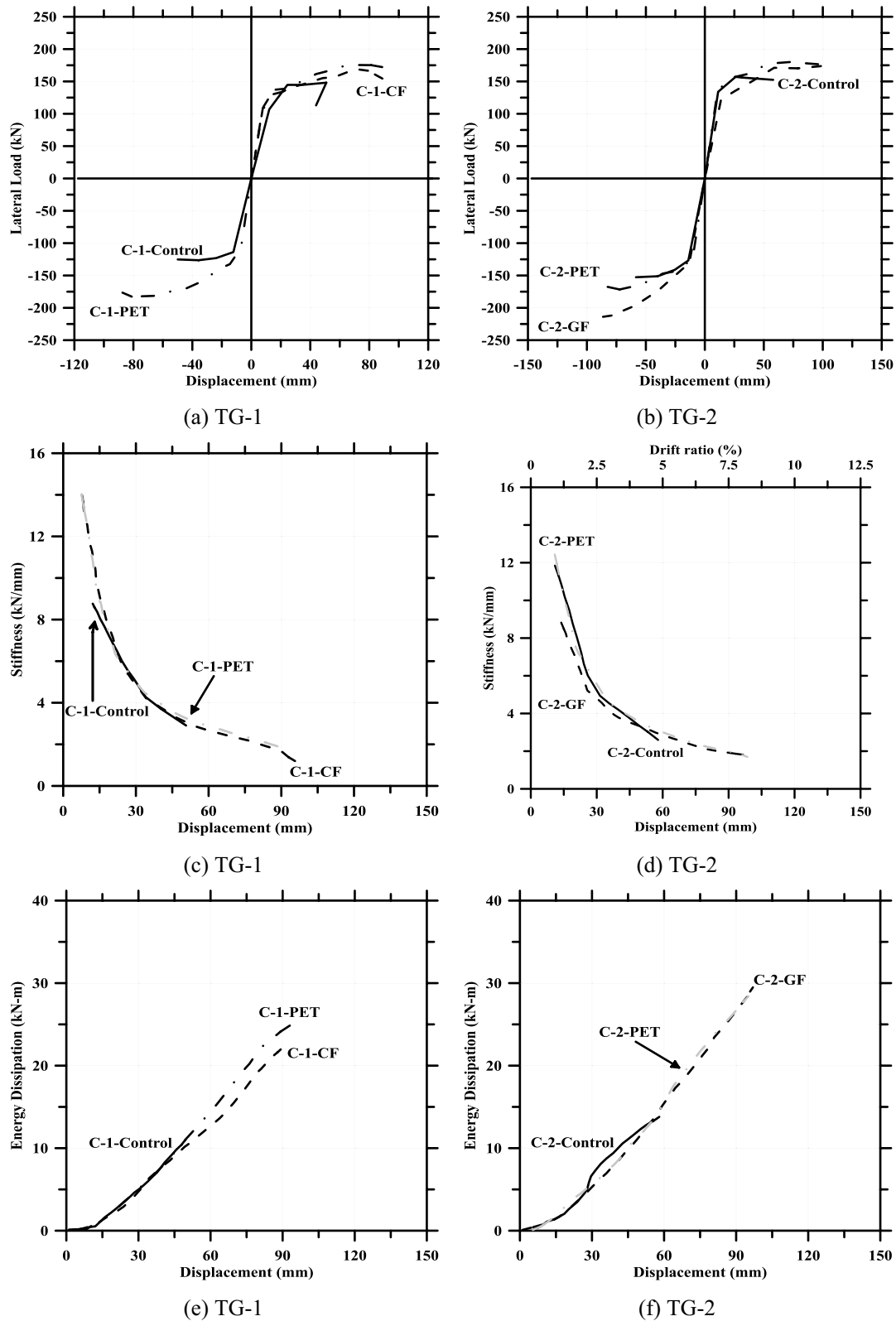


Fig. 10 Envelop, stiffness, and energy dissipation of TG-1 and TG-2 columns.

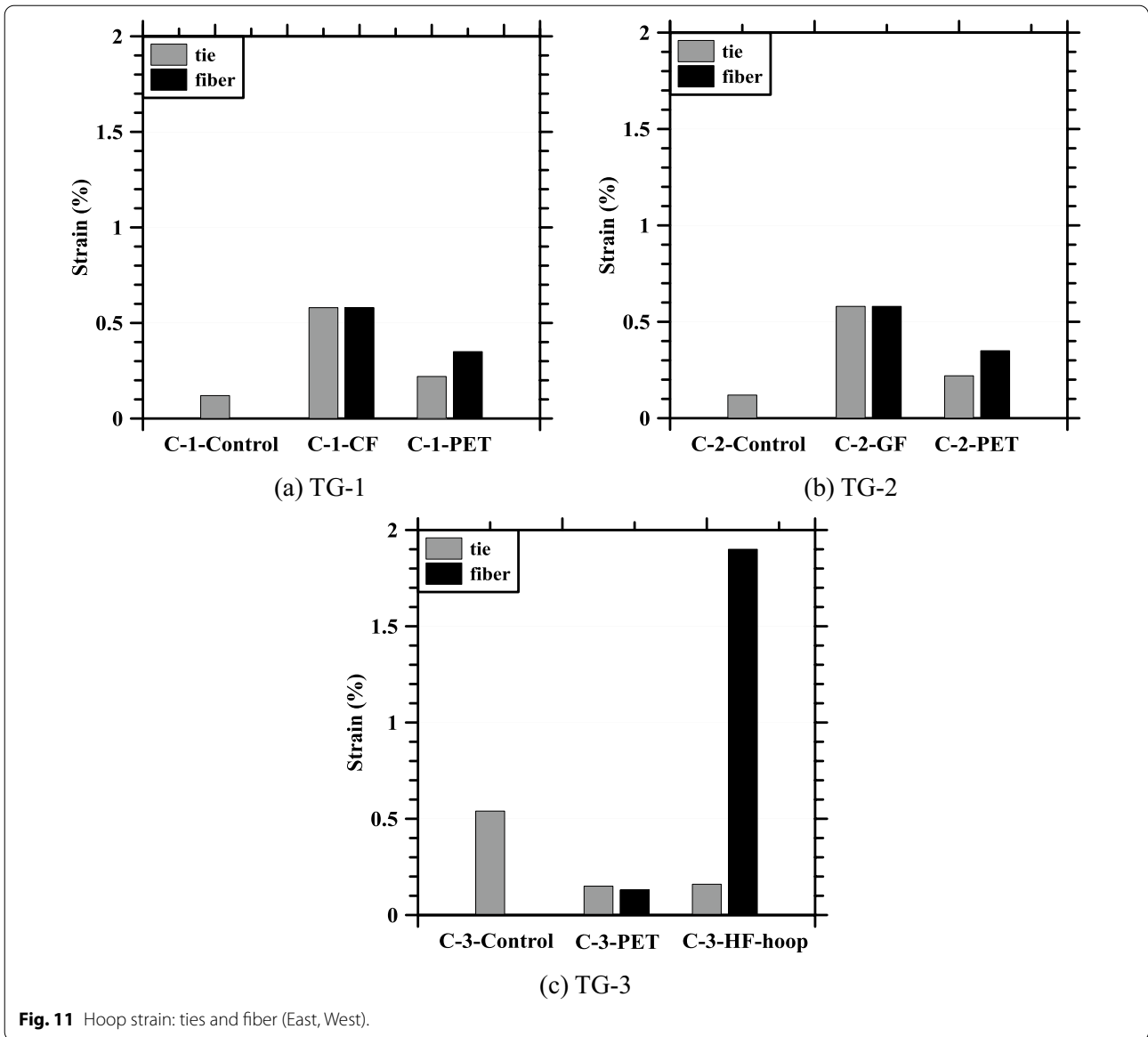


Fig. 11 Hoop strain: ties and fiber (East, West).

for simulating the strain-softening behavior. The simple relationship is as follows:

$$f'_{cc} = f'_{co} + k_1 f_l \tag{1}$$

$$\varepsilon_{cc} = \varepsilon_{co} \left(1 + k_2 \frac{f_l}{f'_{co}} \right) \tag{2}$$

where f'_{cc} and ε_{cc} are the maximum concrete stress and the corresponding strain, respectively, under the lateral fluid pressure f_l ; f'_{co} and ε_{co} are unconfined concrete strength and corresponding strain, respectively; and k_1, k_2 are coefficients that are functions of the concrete mixture and the lateral pressure.

In Eqs. (1) and (2), k_1 and k_2 are assumed to be 4.1 and 5 k_1 , respectively (Richart et al., 1928). The hydrostatic pressure f_l in concrete confined by FRP with linear elastic stress–strain behavior, such as CF and GE, can be determined using the following equation:

$$f_l = \frac{2E_f n t_f \varepsilon_{fe}}{D} \tag{3}$$

where E_f is the elastic modulus of FRP, n is the number of FRP layers, t_f is the thickness of one layer of FRP, ε_{fe} is the effective strain of FRP at failure, and D is the diameter of the circular concrete section.

In the case of PET with non-linear stress–strain behavior, Eq. (4) can be used:

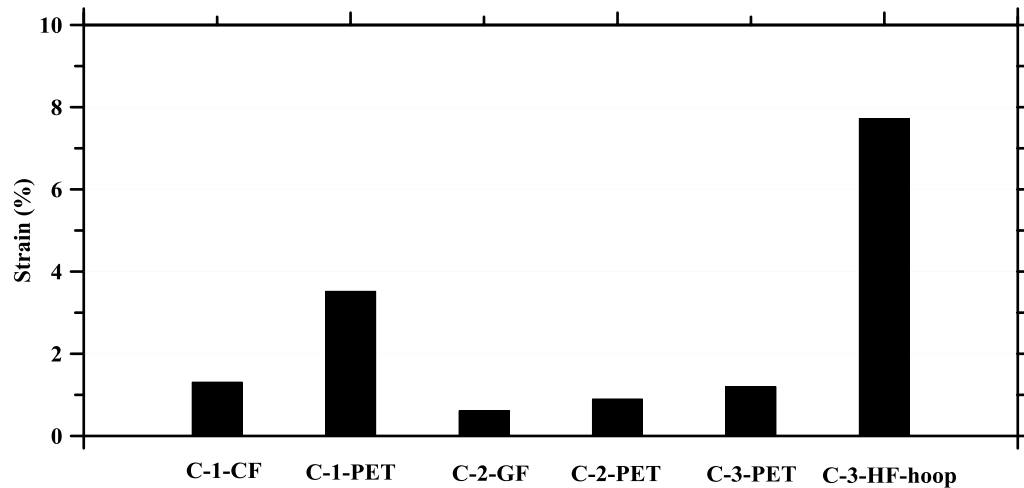


Fig. 12 Fiber strain (hoop strain of extreme compression fiber).

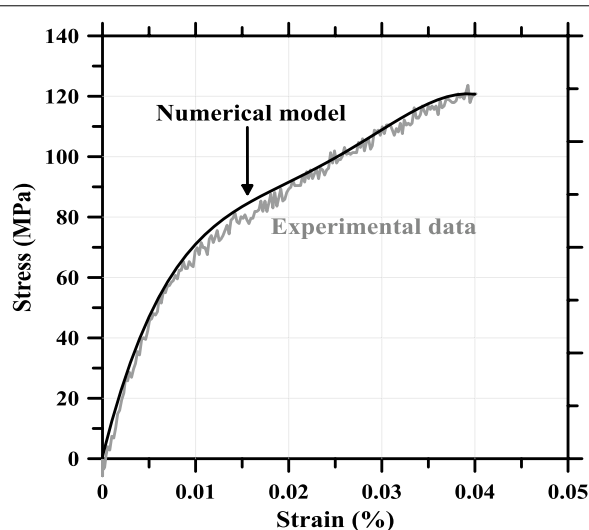


Fig. 13 PET stress–strain relationship (up to 4% strain).

$$f_t = \frac{2f_f n t_f}{D} \quad (4)$$

where f_f is stress of the FRP at the effective strain (ϵ_{fe}).

The stress–strain relationship of PET is non-linear, as depicted in Fig. 1. A numerical expression (a polynomial equation) was developed using the least square method to determine the best fit curve up to 4% PET strain, as presented in Fig. 13. A bi-linear relationship of reinforcement (including strain hardening) was used based on the actual test results of the reinforcing bars used for the column test. Fig. 14 shows the stress–strain relationship of various concretes confined by different FRPs for all columns determined using the theoretical model by Mander et al. (1988). Fig. 14a shows the stress–strain behavior

of TG-1 concretes C-1-Control, and C-1-CF and C-1-PET confined by CF and PET, respectively. The concrete confined by 20 layers of PET (C-1-PET) had the highest strength and ultimate strain. Both strength and ultimate strain also increased for concrete confined by one layer of CF (C-1-CF), but the strength was lower, and the ultimate strain was significantly smaller than C-1-PET. By contrast, in Fig. 14b, the concrete confined by 1 layer of GF (C-2-GF) had the highest strength, whereas the concrete confined by 10 layers of PET (C-2-PET) exhibited the highest ultimate strain. Fig. 14c shows that the confinement effect of 1 layer of the HF strand (C-3-HF) was not as good as 25 layers of PET (C-3-PET). Overall, the strength and ultimate strain of the FRP-confined concretes were significantly higher than those of the control.

4.2 Section Analysis

The stress–strain behaviors shown in Fig. 14 should be directly related to the moment capacity of the section and the curvature ductility. Moment–curvature analyses were carefully performed using the behavior of confined concretes, as determined above. We also used actual material properties of the bi-axial PET sheet and HF strand in terms of numerical models for HF strand and PET demonstrated in Figs. 9 and 14, respectively, and bi-linear stress–strain behavior of reinforcement, including strain hardening. Table 5 summarizes the results for the TG-3 columns.

According to Table 5, the analytically determined flexural strengths and the experimental results match well, especially at ultimate state. The predicted flexural strengths overestimated the actual strength by about 10% or less. For C-3-PET, the bi-axially woven PET sheet not only had fibers stretched in the hoop direction, but the

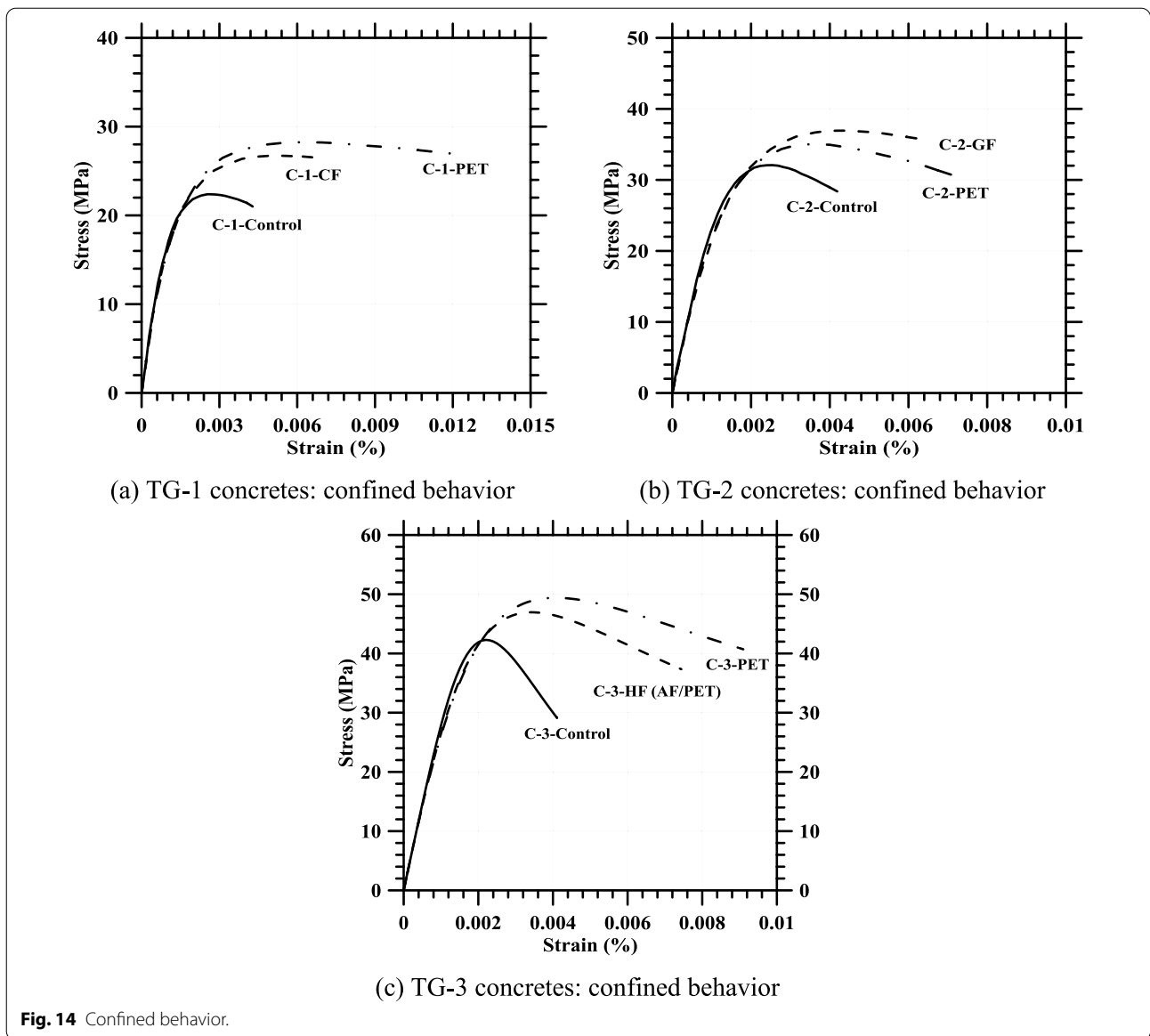


Fig. 14 Confined behavior.

Table 5 Results of moment–curvature analyses versus test results: TG-3 columns.

Column index	Test results moment (kNm)		Analysis results moment (kNm), curvature (10^{-5} rad/mm)				M_{y_calc}/M_{y_test} (%)	M_{u_calc}/M_{u_test} (%)	Curvature ductility Φ_u/Φ_y
	M_{y_test}	M_{u_test}	Yield		Ultimate				
			M_{y_calc}	Φ_y	M_{u_calc}	Φ_u			
C-3-control	183	199	150	1.12	192	3.38	82.0	96.3	3.0
C-3-PET (hoop fibers only)	166	238	152	1.14	213	7.87	91.4	89.4	6.9
C-3-PET (hoop + axial fibers)			153	1.14	223	7.68	92.0	93.5	6.7
C-3-HF-hoop	173	210	149	1.13	200	6.64	86.4	95.5	5.7
C-3-HF-spiral	166	233					89.7	86.1	

M_{y_test} is measured moment at yield stage; M_{u_test} is measured moment at ultimate stage; M_{y_calc} is theoretical momenta at yield stage; Φ_y is theoretical curvature of column at yield stage; M_{u_calc} is theoretical momenta at ultimate stage; Φ_u is theoretical curvature of column at ultimate stage.

axial fibers were also tensed when the retrofitted column was subjected to flexure. Therefore, the contribution of the axial fibers to the flexural strength was determined for C-3-PET with the results included in Table 5, which indicates that the role of axial fibers in increasing flexural strength was not significant. The section curvature ductility increased from 3.0 for the control to over 5–6% for the retrofitted columns. The results shown in Table 5 demonstrate that it is possible to theoretically and accurately predict the strength and ductility of RC columns retrofitted by fibers with non-linear material properties, such as PET.

5 Conclusions

In this research, 11 RC circular columns were built and reinforced by CF, GE, AF, PET, and HF, and a pseudo-seismic test was performed to investigate the effectiveness of structural seismic retrofitting. The following conclusions were reached based on the experimental results and extensive analyses:

1. In TG-1, compared with the control specimen, the ultimate moment of columns confined by CF and PET was improved by 21% and 28%, respectively, and the displacement ductility of specimens wrapped by CF and PET was increased by 130% and 211%, respectively. Due to the improvement in the ultimate moments and ductility of PET, there was no fiber rupture at the ultimate step, whereas CF rupture was clearly observed at the final stage. Even though the PET amount used was approximately 50% of CF in terms of fiber axial stiffness, the ultimate moment of the column reinforced by PET was higher than that of the CF confined specimen because of the higher ultimate strength and strain of the concrete column wrapped by PET.
2. In TG-2, although 1 layer of GF sheet and 10 layers of PET sheet were used for reinforcement of columns, signifying that fiber axial stiffness of PET was about 50% of GE, ductility of PET wrapped column was higher than that of column confined by GF due to the high tensile ductility of PET. However, the flexural strength of the PET wrapped column was slightly lower than that of the GF reinforced column. When compared with the control column, the ultimate moment of specimens reinforced by GF and PET increased by 11% and 15%, respectively, and the displacement ductility of columns confined by GF and PET increased by 38% and 75%, respectively.
3. In TG-3, based on the control specimen, the ultimate moment of PET, HF hoop, and HF-spiral wrapped columns was increased by 24%, 13%, and 23%, respectively, and the displacement ductility of speci-

mens confined by PET, HF hoop, and HF-spiral was improved by 194%, 185%, and 175%, respectively. A comparison of the columns reinforced by PET, HF-hoop, and HF-spiral revealed that their ultimate moment and strain were close to each other. Thus, regardless of the different wrapping methods, such as hoop and spiral, there was no difference between the specimens in terms of seismic performance; one layer of HF sheet with hoop or spiral wrapping had almost the same lateral confinement effect as 25 layers of PET sheet. Despite the low elastic modulus of PET, the RC column with lap-spliced main bars demonstrated a similar level of strength and ductility as the RC column with straight bars, while both columns were strengthened by HF wrapping in a spiral fashion.

4. All three different fibers, that is, GE, CF, and PET, and the AF and PET hybrid FRP, were effective in terms of strength and ductility. We observed that the final failure mode of the CF- or GF-wrapped column was rupture, followed by main bar buckling. Although the PET retrofitted column demonstrated ductile behavior in terms of displacement and drift ratio, the disadvantage was that a large amount of PET had to be used because of its low elastic modulus (about 1/20th of CF elastic modulus). Based on the test results of TG-3, HF was presented as an alternative fiber that can overcome the shortcoming of PET. The durability of PET is currently being investigated to evaluate its field applicability.

Acknowledgements

Not applicable.

Authors' contributions

DC: conceptualization, methodology, validation, formal analysis, investigation, resources, data curation, writing—original draft preparation, writing—review and editing, visualization, supervision, project administration, funding acquisition; SH: writing—original draft preparation, writing—review and editing, visualization, project administration, funding acquisition; M-KL: formal analysis, investigation, data curation; S-SH: formal analysis, investigation; SV: data curation. All authors have read and agreed to the published version of the manuscript. All authors read and approved the final manuscript.

Authors' information

Donguk Choi, Ph.D., Professor, School of Architecture and Design Convergence, Hankyong National University, Anseong, Gyeonggi, Korea; Seongwon Hong, Ph.D., Associate Professor, Department of Safety Engineering, Korea National University of Transportation, Chungju, Chungbuk, Korea (Corresponding Author: shong@ut.ac.kr); Myung-Kwan Lim, Ph.D., Professor, Department of Architectural Engineering, Songwon University, Gwangju, Korea; Sang-Su Ha, Ph.D., Professor, Department of Architectural Engineering, Kangnam University, Youngin, Gyeonggi, Korea; Sorrasak Vachirapanyakun, Former Graduate Student, Graduate School of Architecture, Hankyong National University, Anseong, Gyeonggi, Korea.

Funding

This research was supported by Basic Science Research Program through the National Research Foundation of Korea funded by the Ministry of Education

(No. 2021R1A4A2001964) and by the Young Researcher Program through the National Research Foundation of Korea funded by Ministry of Science, ICT & Future Planning (No. 2021R1C1C1010087). The views expressed are those of authors, and do not necessarily represent those of the sponsors.

Availability of data and materials

The data sets used and analyzed in this study are all included in the manuscript, figures, and tables.

Declarations

Competing interests

The authors declare that they have no known competing financial interests or personal relationships that could have appeared to influence the work reported in this paper.

Author details

¹School of Architecture and Design Convergence, Hankyong National University, Anseong, Gyeonggi, Korea. ²Department of Safety Engineering, Korea National University of Transportation, Chungju, Chungbuk, Korea. ³Department of Architectural Engineering, Songwon University, Gwangju, Korea. ⁴Department of Architectural Engineering, Kangnam University, Youngin, Gyeonggi, Korea. ⁵Graduate School of Architecture, Hankyong National University, Anseong, Gyeonggi, Korea.

Received: 10 June 2021 Accepted: 9 November 2021

Published online: 23 November 2021

References

- American Concrete Institute Committee 440. (2003). Guide for the Design and Construction of Concrete Reinforced with FRP Bars (ACI 440-1R-03). ACI, pp. 42.
- American Concrete Institute Committee 440. (2007). Report on Fiber-Reinforced Polymer (FRP) Reinforcement for Concrete Structures (ACI PRC-440-07). ACI.
- American Society for Testing and Materials International. (2008). Standard test method for tensile properties of plastic (ASTM D638-08). ASTM, pp. 16.
- Anggawidjaja, D., Ueda, T., Dai, J., & Nakai, H. (2006). Deformation capacity of RC piers wrapped by new fiber-reinforced polymer with large fracture strain. *Cement and Concrete Composites*, 28, 914–927. <https://doi.org/10.1016/j.cemconcomp.2006.07.011>
- Cao, V. V., & Pham, S. Q. (2019). Comparison of CFRP and GFRP wraps on reducing seismic damage of deficient reinforced concrete structures. *International Journal of Civil Engineering*, 17, 1667–1681.
- Choi, D. U., Kang, T. H. K., Ha, S. S., Kim, K. H., & Kim, W. S. (2011). Flexural and bond behaviour of concrete beams strengthened with hybrid carbon-glass fiber-reinforced polymer sheets. *ACI Structural Journal*, 108, 90–98.
- American Concrete Institute. (2013). Guide for Testing Reinforced Concrete Structural Elements under Slowly Applied Simulated Seismic Loads (374.2R-13) ACI, pp. 18.
- Dai, J. G., Lam, L., & Ueda, T. (2012). Seismic retrofit of square RC columns with polyethylene terephthalate (PET) fibre reinforced polymer composites. *Construction and Building Materials*, 27, 206–217. <https://doi.org/10.1016/j.conbuildmat.2011.07.058>
- Fahmy, M. F. M., & Wu, Z. (2010). Evaluating and proposing models of circular concrete columns confined with different FRP composites. *Composite: Part B Engineering*, 41, 199–213. <https://doi.org/10.1016/j.compositesb.2009.12.001>
- International Standard Organization. (2015). Fibre-reinforced polymer (FRP) reinforcement of concrete—Test methods—part 2: FRP sheets (10406-2) ISO, pp.11.
- Korea Concrete Institute. (2012). Korea Structural Concrete Design Code 2012. KCI.
- Liu, J., & Sheikh, S. A. (2013). Fiber-reinforced polymer-confined circular columns under simulated seismic loads. *ACI Structural Journal*, 110, 941–952.
- Liu, X., & Li, Y. (2018). Experimental study of seismic behavior of partially corrosion-damaged reinforced concrete columns strengthened with FRP composites with large deformability. *Construction and Building Materials*, 191, 1071–1081. <https://doi.org/10.1016/j.conbuildmat.2018.10.072>
- Mander, J. B., Priestly, M. J. N., & Park, R. (1988). Theoretical stress-strain model for confined concrete. *Journal of the Structural Engineering. American Society of Civil Engineers*, 114, 1804–1826.
- Manders, P. W., & Bader, M. G. (1981). The strength of hybrid glass/carbon fibre composites: part 1 Failure strain enhancement and failure mode. *Journal of Materials Science*, 16, 2233–2245.
- Mhanna, H. H., Hawileh, R. A., Abuzaid, W., Naser, M. Z., & Abdalla, J. (2020). Experimental investigation and modeling of the thermal effect on the mechanical properties of polyethylene-terephthalate FRP laminates. *Journal of Materials in Civil Engineering*, 32(10), 04020296.
- Mirmiran, A., Shahawy, M., Samaan, M., Echary, H. E., Mastrapa, J. C., & Pico, O. (1998). Effect of column parameters on FRP-Confined Concrete. *Journal of Composites for Construction*. [https://doi.org/10.1061/\(ASCE\)1090-0268\(1998\)2:4\(175\)](https://doi.org/10.1061/(ASCE)1090-0268(1998)2:4(175))
- Naser, M. Z., Hawileh, R. A., & Abdalla, J. A. (2019). Fiber-reinforced polymer composites in strengthening reinforced concrete structures: a critical review. *Engineering Structures*, 198, 109542.
- Parghi, A., & Alam, M. S. (2017). Seismic collapse assessment of non-seismically designed circular RC bridge piers retrofitted with FRP composites. *Composite Structures*, 160(15), 901–916.
- Obaidat, Y.T., Ashteyat, A.M., Obaidat, A., Abu-Lebdeh, M.N. (2021), "Bond characteristics between concrete and near-surface mounted carbon fiber reinforced polymer cords. *Journal of Structural Integrity and Maintenance* 6(4):223-236. <https://doi.org/10.1080/24705314.2021.1950379>
- Richart, F.E., Brandtzaeg, A., Brown, R.L. (1928). A study of the failure of concrete under combined compressive stress. Bulletin 190, Univ. of Illinois Engineering Experimental Station.
- Saleem, S., Pimanmas, A., & Rattanapitikon, W. (2018). Lateral response of PET-FRP-confined concrete. *Construction and Building Materials*, 159, 390–407. <https://doi.org/10.1016/j.conbuildmat.2017.10.116>
- Ueda, T., Dai, J., & Sato, Y. (2006). Unified analytical approaches for determining shear bond characteristics of FRP-concrete interfaces through pullout tests. *Journal of Advanced Concrete Technology*. <https://doi.org/10.3151/jact.4.133>
- Youssf, O., ElGawady, M., & Mills, J. E. (2015). Displacement and plastic hinge length of FRP-confined circular reinforced concrete columns. *Engineering Structures*, 101, 465–476.
- Zhang, D., Zhao, Y., Jin, W., Ueda, T., & Nakai, H. (2017). Shear strengthening of corroded reinforced concrete columns using pet fiber-based composites. *Engineering Structures*, 153, 757–765. <https://doi.org/10.1016/j.engstruct.2017.09.030>
- Zhou, S. C., Demartino, C., Xu, J. J., & Xiao, Y. (2021). Effectiveness of CFRP seismic-retrofit of circular RC bridge piers under vehicular lateral impact loading. *Engineering Structures*, 243(15), 112602. <https://doi.org/10.1016/j.engstruct.2021.112602>

Publisher's Note

Springer Nature remains neutral with regard to jurisdictional claims in published maps and institutional affiliations.

Submit your manuscript to a SpringerOpen[®] journal and benefit from:

- Convenient online submission
- Rigorous peer review
- Open access: articles freely available online
- High visibility within the field
- Retaining the copyright to your article

Submit your next manuscript at ► [springeropen.com](https://www.springeropen.com)